Neutron Skins in Exotic Nuclei from Skyrme Hartree-Fock Calculations

P. Sarriguren[1], M. K. Gaidarov[1,2], E. Moya de Guerra[3,1], and A. N. Antonov[2]

[1] Instituto de Estructura de la Materia, CSIC, Serrano 123, 28006 Madrid, Spain
[2] Institute for Nuclear Research and Nuclear Energy, Bulgarian Academy of Sciences, 1784 Sofia, Bulgaria
[3] Departamento de Fisica Atomica, Molecular y Nuclear, Facultad de Ciencias Fisicas, Universidad Complutense de Madrid, Madrid E-28040, Spain

Abstract. The formation of neutron skin and its evolution with an increase of the neutron number is investigated within a self-consistent framework based on deformed Hartree-Fock calculations with density dependent Skyrme forces and pairing correlations in BCS approximation. We study several isotopic chains of Ni, Kr, and Sn nuclei and consider all the experimentally observed isotopes from neutron-deficient to neutron-rich. Various definitions of the neutron skin thickness based on the differences between neutron and proton radii as well as on comparison of the tails of the neutron and proton density distributions have been tested. The effects of deformation on the neutron skins in even-even deformed nuclei based on the example of Kr isotopes are discussed.

1 Introduction

The determination of charge radii and extraction of nuclear matter radii are crucial for studying the evolution of neutron and proton skins along isotopic chains. To get information on the neutron skin thickness one needs data obtained with probes having different sensitivities to the proton and neutron distributions. The methods for extracting the neutron skin thickness mostly include hadron scattering [1, 2], antiprotonic atoms [3], parity violating electron scattering [4–6], as well as giant dipole resonance method [7] and spin-dipole resonance method [8, 9].

On the theoretical side, calculations of nuclear charge and matter radii of exotic nuclei are usually made in the framework of mean-field approaches, namely Hartree-Fock (HF) method or Hartree-Fock-Bogoliubov (HFB) method including pairing correlations (*e.g.*, Ref. [10]). Recently, the self-consistent relativistic mean-field (RMF) model has been widely applied to both stable and unstable nuclei (*e.g.*, Ref. [11]). Many calculations show that the RMF model can reproduce with good precision a number of ground-state nuclear properties including the charge radii [12]. The charge rms radii were successfully described very recently in Ref. [10], where a generator coordinate method (GCM) on top of Gogny HFB calculations was explored.

Theoretical identification of skin structure in neutron-rich weakly bound nuclei, however, is still a matter of discussion. In Ref. [13] a definition of the neutron skin

and its appearance were presented in terms of spherical HF calculations. The proposed criteria which deal with proton and neutron densities allowed one to predict neutron skins in nuclei far from the β stability line. The Helm model [14, 15] has been applied in Ref. [16] to analyze neutron and proton skins, as well as halos, of even-even Ni, Sn, and Pb isotopes in terms of form factors.

In the present study (as well as in Ref. [17]), the properties of even-even Ni (A=48–78), Kr (A=70–100), and Sn (A=100–136) isotopes are described using the deformed self-consistent mean-field Skyrme HF+BCS method. We choose some medium and heavy Ni, Kr, and Sn isotopes because many of these sets, which lie in the nuclear chart between the proton and neutron drip lines can be formed as radioactive ions to perform scattering experiments. The main goal of this study is to clarify theoretically the emergence of the neutron and proton skins in neutron-rich and neutron-deficient isotopes, respectively, by testing different definitions for the skin thickness in the framework of the deformed Skyrme HF+BCS model. Alternatively to one of the criteria for the neutron skin proposed in Ref. [13] we consider another one which treats proton and neutron densities in a similar way. The calculated charge rms radii are compared with the laser or muonic atoms spectroscopy measurements of isotope shifts performed on Sn [18–21], Ni [22, 23], and Kr [24] isotopes. The neutron skin thicknesses obtained in this paper are compared with the available experimental data extracted from methods mentioned above for even-even Sn isotopes with masses from 112 to 124. We also study whether the emergence of a skin is influenced by the nuclear shape, an issue that has not been sufficiently studied so far. The question of skin formation in nuclei having a non-spherical shape is discussed in detail on the example of Kr isotopes, assuming axial symmetry.

2 Theoretical Formalism

The results discussed in this paper have been obtained from self-consistent deformed Hartree-Fock calculations with density dependent Skyrme interactions [25] and pairing correlations. Pairing between like nucleons has been included by solving the BCS equations at each iteration either with a fixed pairing gap parameter (determined from the odd-even experimental mass differences) or with a fixed pairing strength parameter. We consider the Skyrme force SLy4 [26]. We also show in some instances the results obtained from other parametrizations, namely Sk3 [27] and SG2 [28] because they are among the most extensively used Skyrme forces and are considered as standard references.

The spin-independent proton and neutron densities are given by

$$\rho(\vec{R}) = \rho(r,z) = \sum_i 2v_i^2 \rho_i(r,z)\,, \tag{1}$$

in terms of the occupation probabilities v_i^2 resulting from the BCS equations and the single-particle densities ρ_i. The multipole decomposition of the density can be written as [25]

$$\rho(r,z) = \sum_{\lambda} \rho_{\lambda}(R) P_{\lambda}(\cos\theta) = \rho_0(R) + \rho_2(R)\, P_2(\cos\theta) + \dots \,, \tag{2}$$

with multipole components λ

$$\rho_{\lambda}(R) = \frac{2\lambda+1}{2} \int_{-1}^{+1} P_{\lambda}(\cos\theta)\rho(R\cos\theta, R\sin\theta) d(\cos\theta)\,, \tag{3}$$

and normalization given by

$$\int \rho(\vec{R}) d\vec{R} = X; \qquad 4\pi \int R^2 dR \rho_0(R) = X\,, \tag{4}$$

with $X = Z,\ N$ for protons and neutrons, respectively.

The mean square radii for protons and neutrons are defined as

$$< r^2_{\rm p,n} >= \frac{\int R^2 \rho_{\rm p,n}(\vec{R}) d\vec{R}}{\int \rho_{\rm p,n}(\vec{R}) d\vec{R}}\,, \tag{5}$$

and the rms radii for protons and neutrons are simply given by

$$r_{\rm p,n} =< r^2_{\rm p,n} >^{1/2}\ . \tag{6}$$

The mean square radius of the charge distribution in a nucleus can be expressed as

$$< r^2_{\rm ch} >=< r^2_{\rm p} > + < r^2_{\rm ch} >_{\rm p} + (N/Z) < r^2_{\rm ch} >_{\rm n} + r^2_{\rm CM} + r^2_{\rm SO}\,, \tag{7}$$

where $< r^2_{\rm p} >$ is the mean square radius of the point proton distribution in the nucleus (5), $< r^2_{\rm ch} >_{\rm p}$ and $< r^2_{\rm ch} >_{\rm n}$ are the mean square charge radii of the charge distributions in a proton and a neutron, respectively. $r^2_{\rm CM}$ is a small correction due to the center of mass motion, which is evaluated assuming harmonic-oscillator wave functions. The last term $r^2_{\rm SO}$ is a tiny spin-orbit contribution to the charge density. Correspondingly, we define the charge rms radius

$$r_{\rm c} =< r^2_{\rm ch} >^{1/2}\ . \tag{8}$$

To study the neutron skin thickness we will use first the difference between the neutron and proton rms radii to characterize the different spatial extensions of neutron and proton densities. But a more effective tool to analyze skins [16] is the Helm model [14, 15]. This is a model that allows one to extract from the form factor in a simple way the two main characteristics of the density, a diffraction radius and a surface thickness. In this model one describes the density by convoluting a hard sphere (hs) density having diffraction radius R_d with a gaussian of variance σ,

$$\rho_{\rm Helm}(r; R_d, \sigma) = \rho_{\rm hs}(r; R_d) * \rho_G(r; \sigma)\,, \tag{9}$$

where

$$\rho_{\rm hs}(r,R_d)=\frac{3X}{4\pi R_d^3}\Theta(R_d-r), \tag{10}$$

and

$$\rho_G(r;\sigma)=(2\pi\sigma^2)^{-3/2}e^{(-r^2/2\sigma^2)}. \tag{11}$$

The corresponding Helm form factor is

$$F_{\rm Helm}(q)=F_{\rm hs}(q;R_d)F_G(q;\sigma)=\frac{3}{qR_d}j_1(qR_d)e^{-\sigma^2q^2/2}\,. \tag{12}$$

Now, the most prominent feature of the density distribution, namely its extension, can be related to the first zero in the form factor, this is the diffraction radius

$$R_d=4.49341/q_1\,, \tag{13}$$

where q_1 is the first zero of the form factor. The nuclear surface width σ can be related to the height of the second maximum of the form factor located at $q_{\rm max}$:

$$\sigma^2=\frac{2}{q_{\rm max}^2}\ln\frac{3j_1(q_{\rm max}R_d)}{R_dq_{\rm max}F(q_{\rm max})}\,. \tag{14}$$

Taking into account that the second moment of a convoluted distribution is given by the sum of the second moments of the two single distributions, one gets the Helm rms radius

$$R_{\rm rms}^{\rm Helm}=\sqrt{\frac{3}{5}\,(R_d^2+5\sigma^2)}\,. \tag{15}$$

Taking out the factors $\sqrt{3/5}$, which relate the rms radii to the radii of the equivalent uniform hard spheres, we define

$$R_{\rm hs}=\sqrt{5/3}<r^2>^{1/2} \tag{16}$$

and

$$R_{\rm Helm}=\sqrt{5/3}\,R_{\rm rms}^{\rm Helm}=\sqrt{R_d^2+5\sigma^2}\,. \tag{17}$$

From these definitions we construct the following neutron-proton radius differences that will be used:

$$\Delta R_d=R_d(n)-R_d(p)\,, \tag{18}$$

$$\Delta R_{\rm hs}=R_{\rm hs}(n)-R_{\rm hs}(p)=\sqrt{5/3}\left[<r_n^2>^{1/2}-<r_p^2>^{1/2}\right]\,, \tag{19}$$

$$\Delta R_{\rm Helm}=R_{\rm Helm}(n)-R_{\rm Helm}(p)\,. \tag{20}$$

3 Results

Beginning with Sn isotopes for which more data and calculations are available, we show on the right panel of Figure 1 our results for the squared charge radii differences in Sn isotopes obtained from three different Skyrme forces, SLy4, SG2

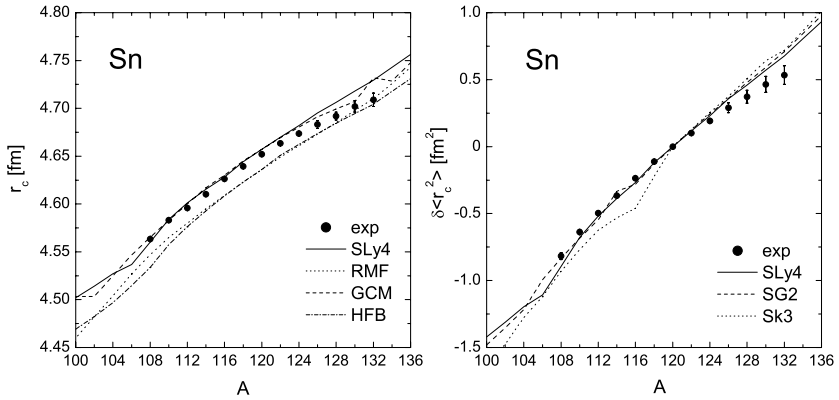

Figure 1. Left panel: Charge rms radii r_c of tin isotopes. The SLy4 result is compared with the results from RMF calculations [11], HFB [10] and GCM [10]. Experimental data are from [18–21]; Right panel: Theoretical (with different Skyrme forces) and experimental isotope shifts $\delta\langle r_c^2\rangle$ of tin isotopes relative to ^{120}Sn.

and Sk3. We compare them to experiment, taking the radius of ^{120}Sn as the reference [21]. On the left panel we compare our SLy4 results for the charge radii with the other theoretical approaches mentioned above. The general purpose of Figure 1 is firstly to show that different Skyrme forces do not differ much in their predictions of charge rms radii and secondly, to show that our results with SLy4 are comparable to other theoretical predictions including approaches that go beyond the mean-field approximation, as well as relativistic approaches. We conclude that our method reproduces the experimental data with a similar accuracy to other microscopic calculations that, as explained above, may be more sophisticated but may also be more time consuming. This agreement provides a good starting point to make predictions for other quantities such as neutron-proton radii differences, where the experimental information is scarce and it is not as accurate as in the case of charge radii.

In Figure 2 we plot the differences between the rms of neutrons and protons $\Delta r_{np} = r_n - r_p$. On the left panel we show our results for Sn isotopes and compare them to RMF results and to experimental data. As we can see the experimental data are located between the predictions of both theoretical approaches and in general, there is agreement with experiment within the error bars. On the right panels we see the predictions for Δr_{np} in the cases of Ni and Kr isotopes, where there are no data. As it can be seen, the RMF results for the difference Δr_{np} systematically overestimate the Skyrme HF results. The reason for this is related to the difference in the nuclear symmetry energy and, consequently, to the different neutron equation of state (EOS) which has been extensively studied in recent years [29–32].

Figure 3 shows the neutron (solid) and proton (dashed) densities $\rho_0(R)$ (2) in the ^{100,120,136}Sn isotopes. From left to right we see the evolution of these densities as we increase the number of neutrons. In the case of ^{100}Sn (N=Z=50) we see that the two densities are practically the same except for Coulomb effects that make

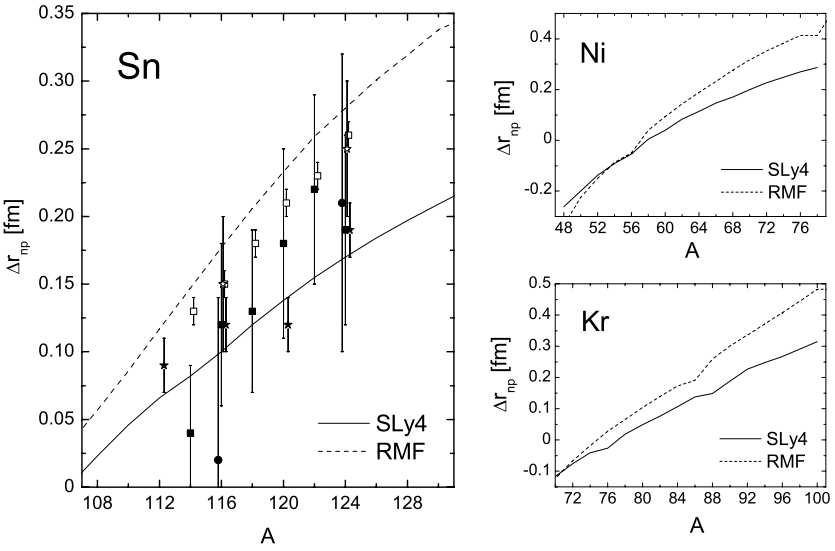

Figure 2. Difference between neutron and proton rms radii Δr_{np} of Sn, Ni, and Kr isotopes calculated with SLy4 force. The RMF calculation results are from Ref. [11]. The experimental data for Sn isotopes measured in (p, p) reaction (open stars) [1, 2], antiproton atoms (full stars) [3], giant dipole resonance method (full circles) [7] and spin dipole resonance method (full and open squares) [8, 9] are also shown.

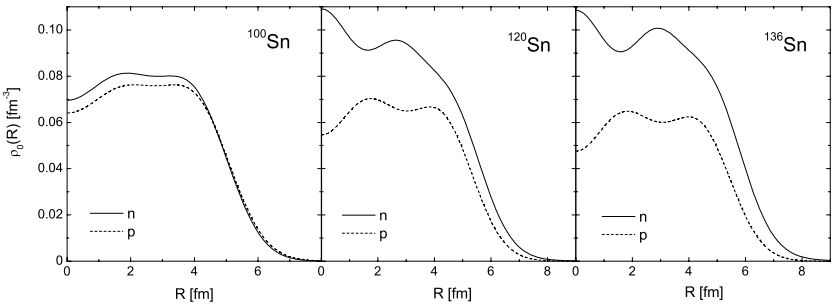

Figure 3. HF+BCS proton and neutron densities $\rho_0(R)$ of ^{100}Sn, ^{120}Sn, and ^{136}Sn calculated with SLy4 force.

the protons to be more extended and, therefore, this has to be compensated with a small depression in the interior. The effect of adding more and more neutrons is to populate and extend the neutron densities. This makes also the proton distribution to follow the neutron one, increasing its spatial extension. The cost of this radius enlargement in the case of protons is a depression in the nuclear interior to preserve the normalization to the constant number of protons $Z = 50$. Then, it can be seen graphically the emergence of a region at the surface where the protons have practi-

cally disappeared while the neutrons still survive. We will quantify later this region in terms of the neutron skin thickness definitions.

The thickness of a neutron skin in nuclei may be defined in different ways. One of these possibilities is to define it as the difference between the root mean square radius of neutrons and that of protons, as we have plotted in Figure 2. Similarly, it can be defined as the difference between the neutron and proton radii of the equivalent uniform spheres [Eq. (19)]. Alternatively, it can be defined as the difference between the neutron and proton diffraction radii (18) or Helm radii (20).

On the other hand, the skin thickness can be also defined in terms of some criteria that the neutron and proton densities must fulfill. In Ref. [13] the neutron skin thickness is defined as the difference between two radii, R_1 and R_2. R_1 is the radius at which the ratio of the neutron density to the proton density is equal to some given value (4 in [13]). R_2 is the radius at which the neutron density becomes smaller than some percentage of the density at the center of the nucleus (1 % in [13]). When this difference, $\Delta R = R_2 - R_1$, is larger than some established value (in [13] this value is 1 fm, which is comparable to the range of the nuclear force), a neutron skin with skin thickness ΔR is said to occur. We have also considered the case where the first criterion for the inner radius R_1 of the neutron skin is changed. We use instead of the above criterion for R_1, the radius at which the proton density becomes smaller than 1% of the latter at the center, which is similar to the criterion used to define the outer radius R_2, but in this case for proton density instead of the neutron density. When we use the conditions in Ref. [13], we call it criterion (a). When we use the alternative condition for R_1, we call it criterion (b).

We show in Figure 4 the results obtained for the neutron skin thickness in Ni isotopes according to the different definitions discussed above. The left panel contains the results for definitions involving directly the difference between neutron and

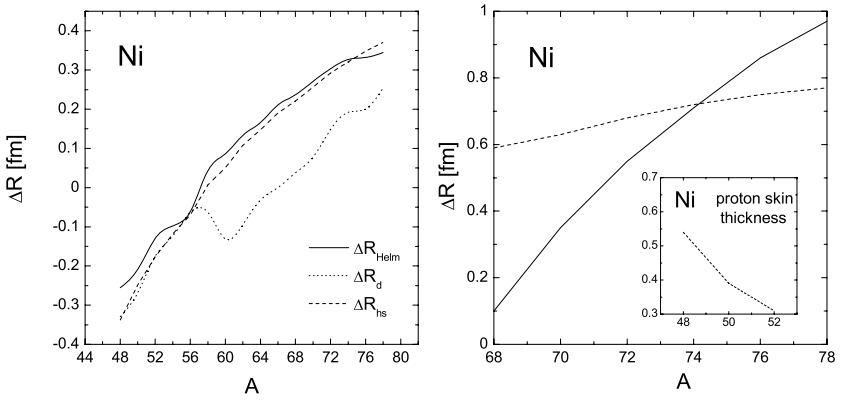

Figure 4. Neutron skin thicknesses for Ni isotopes. Left panel: $\Delta R_{\rm d}$ [Eq. (18)], $\Delta R_{\rm hs}$ [Eq. (19)], and $\Delta R_{\rm Helm}$ [Eq. (20)]; Right panel: corresponding to criterion (a) (solid line) and criterion (b) (dotted line). A formation of proton skin thickness with the criterion (b) is also shown.

proton radii [Eqs. (18)-(20)]. The skin thickness predicted by the difference of the very simple diffraction radii is in general smaller than the thickness predicted by the other two more involved options that are very similar in this range of masses. The right panel contains the neutron skin thickness defined according to the criteria on the density distributions (a) (solid line) and (b) (dashed line). They only differ in the way in which the starting radius of the skin R_1 is chosen. One can see that we obtain larger neutron skin thicknesses when using criterion (b) in the lighter isotopes, but this is reversed for heavier isotopes and we get larger thickness when using criterion (a).

We also consider the most neutron-deficient region of Ni isotopes in a search for the formation of a proton skin. Reversing the definitions of R_1 and R_2 and applying the criterion (b) with protons and neutrons interchanged, the obtained results are shown in the inset of the right panel in Figure 4. We find no proton skin when applying criterion (a). One can see that a small skin starts developing in these isotopes but we cannot push it further because ^{48}Ni is already at the proton drip line. The results are then not conclusive enough to assess the existence of a proton skin in these isotopes.

When the nucleus is deformed, the thickness of the neutron skin might depend on the direction. It is an interesting and natural question to ask whether the deformed densities give rise to a different skin size in the different directions. It is also interesting to know whether the emergence of the skin may be influenced by the nuclear shape. We first study the intrinsic density distributions $\rho(\vec{R})$ in various selected directions. For that purpose we show in Figures 5 and 6 the densities of ^{98}Kr for oblate and prolate shapes, respectively. We can see the spatial distributions for neutrons (solid) and protons (dotted) in three different directions: z-direction $(r = 0)$, r-direction $(z = 0)$, and $r = z$ direction. We can observe that the profiles

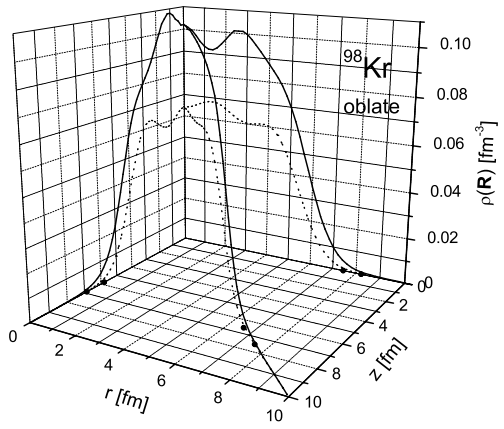

Figure 5. Neutron (solid line) and proton (dotted line) density distributions $\rho(\vec{R})$ in different directions for oblate shape of ^{98}Kr. The full dots shown on the (r, z) plane correspond to radii R_1 and R_2 according to criterion (a).

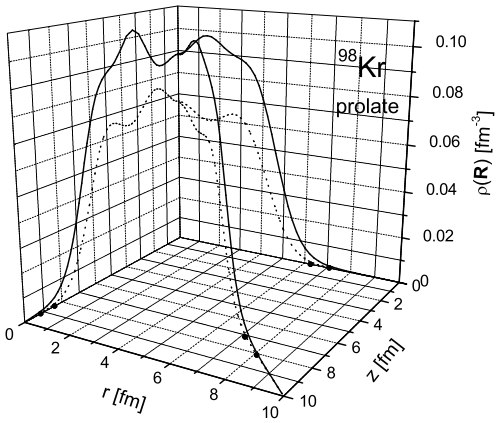

Figure 6. Same as in Figure 5, but for prolate shape of ^{98}Kr.

of the densities as well as the spatial extensions change with the direction. Clearly, the densities are more extended in the z-direction in the case of prolate shapes. The opposite is true in the case of oblate shapes. The case $r = z$ gives always intermediate densities. We have added in the three directions a couple of full dots, indicating the radii R_1 and R_2 that defines the skin thickness according to the above mentioned criterion (a).

It is also worth looking at the points in the (r, z) plane that define the ellipses where the criteria for R_1 and R_2 are met. Figure 7 shows these points for protons (thin lines) and neutrons (thick lines) and for the two shapes, prolate (solid) and

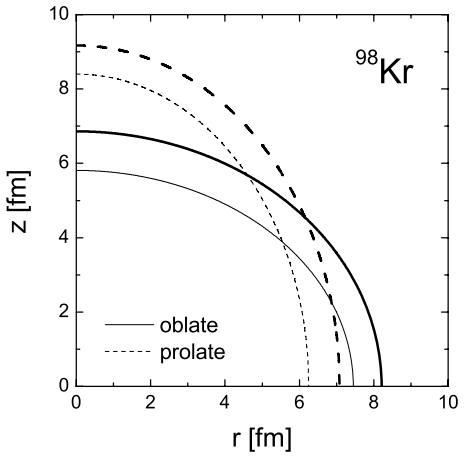

Figure 7. Radii R_1 and R_2 according to criterion (a) for neutrons (thick lines) and protons (thin lines) in ^{98}Kr nucleus (shown in rz plane) corresponding to its oblate (solid lines) and prolate (dashed lines) shape.

oblate (dashed). We can see that the size of the skin changes little with the directions perpendicular to the surface, but shows a tendency to increase on the shorter axis. It is interesting to note that the skin size of the spherical component $\rho_0(R)$ is an intermediate value. The overall skin thickness is also similar in the oblate and prolate equilibrium shapes. From this example we may conclude that the skin thickness does not depend much on the oblate or prolate character of the deformation.

4 Conclusions

For the first time the various definitions which have been previously proposed to determine the neutron skin thickness, involving both matter radii and tails of nuclear densities, have been compared within a deformed Skyrme HF+BCS model. Three Skyrme parametrizations have been involved in the calculations: SG2, Sk3 and SLy4. Most of the results shown in the paper are obtained with SLy4 force, but the other Skyrme interactions produce similar results. We find that all definitions of the neutron skin predict to a different extent the existence of a skin in nuclei far from the stability line. Particularly, a pronounced neutron skin can be attributed to heavier isotopes of the three chains considered, namely with $A > 132$ for Sn, $A > 74$ for Ni, and $A > 96$ for Kr isotopes. We also find that for a given isotopic chain the increase of the skin with the neutron number in the neutron-rich nuclei exhibits a rather constant slope, which is different depending on the definition of nuclear skin. More significant neutron skin is obtained when analyzing its formation by means of definition from Ref. [13] (called criterion (a)) or using an alternative one (called criterion (b)). In this case we get an absolute size of the skin larger than 0.4 fm and almost reaching 1 fm for the heaviest isotopes (in the case of criterion (a)). At the same time, the neutron skin determined by the difference between neutron and proton radii using diffraction parameters defined in the Helm model shows a more smooth gradual increase with the neutron excess and it is in size of around 0.3–0.4 fm.

We also show on the example of the neutron-deficient Ni isotopes the possibility to find a proton skin in a similar way to the neutron skin. Although the analysis, which was performed in our paper for this case, uses an alternative criterion to that applied in [13], it indicates a situation close to proton skin formation in Ni isotopes very close to the proton drip line. However, the search for the existence of proton skin could be explored in the most proton-rich nuclei approaching the proton drip lines of lighter nuclei, where $Z > N$.

In the present work the effects of deformation on the skin formation are studied in Kr isotopes which are well deformed nuclei. Taking as an example ^{98}Kr and ^{100}Kr isotopes, we find that the profiles of the proton and neutron densities, as well as the spatial extensions change with the direction in both oblate and prolate shapes. At the same time, the neutron skin thickness remains almost equal along the different directions perpendicular to the surface. We find a very weak dependence of the neutron skin formation on the character of deformation.

5 Acknowledgements

One of the authors (M.K.G.) is grateful for the warm hospitality given by the CSIC and for support during his stay there from the State Secretariat of Education and Universities of Spain (N/Ref. SAB2005–0012). This work was partly supported by the Bulgarian National Science Fund under Contracts No. Φ–1416 and Φ–1501, and by Ministerio de Educación y Ciencia (Spain) under Contract No. FIS2005–00640.

References

1. L. Ray *et al.*, Phys. Rev. C **19**, 1855 (1979).
2. G. W. Hoffmann *et al.*, Phys. Rev. Lett. **47**, 1436 (1981).
3. A. Trzcinska *et al.*, Phys. Rev. Lett. **87**, 082501 (2001).
4. T. W. Donnelly *et al.*, Nucl. Phys. **A503**,589 (1989).
5. C. J. Horowitz *et al.*, Phys. Rev. C **47**, 826 (1993).
6. D. Vretenar, P. Finelli, A. Ventura, G. A. Lalazissis, and P. Ring, Phys. Rev. C **61**, 064307 (2000).
7. A. Krasznahorkay *et al.*, Nucl. Phys. **A567**, 521 (1994).
8. A. Krasznahorkay *et al.*, Phys. Rev. Lett. **82**, 3216 (1999).
9. A. Krasznahorkay *et al.*, Nucl. Phys. **A731**, 224 (2004).
10. J. Libert, B. Roussiere, and J. Sauvage, Nucl. Phys. **A786**, 47 (2007).
11. G. A. Lalazissis, S. Raman, and P. Ring, At. Data Nucl. Data Tables **71**, 1 (1999).
12. Z. Ren, W. Mittig, B. Chen, and Z. Ma, Phys. Rev. C **52**, R20 (1995).
13. N. Fukunishi, T. Otsuka, and I. Tanihata, Phys. Rev. C **48**, 1648 (1993).
14. R. H. Helm, Phys. Rev. **104**, 1466 (1956).
15. J. Friedrich and N. Voegler, Nucl. Phys. **A373**, 192 (1982); J. Friedrich, N. Voegler, and P.G. Reinhard, Nucl. Phys. **A459**, 10 (1986); D. W. L. Sprung, N. Yamanishi, and D. C. Zheng, Nucl. Phys. **A550**, 89 (1992).
16. S. Mizutori, J. Dobaczewski, G. A. Lalazissis, W. Nazarewicz, and P.-G. Reinhard, Phys. Rev. C **61**, 044326 (2000).
17. P. Sarriguren, M. K. Gaidarov, E. Moya de Guerra, and A. N. Antonov, Phys. Rev. C **76**, 044322 (2007).
18. F. Le Blanc *et al.*, Eur. Phys. J. A **15**, 49 (2002).
19. F. Le Blanc *et al.*, Phys. Rev. C **72**, 034305 (2005).
20. M. Anselment, K. Bekk, A. Hanser, H. Hoeffgen, G. Meisel, S. Goring, H. Rebel, and G. Schatz, Phys. Rev. C **34**, 1052 (1986).
21. C. Piller, C. Gugler, R. Jacot-Guillarmod, L. A. Schaller, L. Schellenberg, H. Schneuwly, G. Fricke, T. Hennemann, and J. Herberz, Phys. Rev. C **42**, 182 (1990).
22. B. Nerlo-Pomorska and B. Mach, At. Data Nucl. Data Tables **60**, 287 (1995).
23. G. Fricke *et al.*, At. Data Nucl. Data Tables **60**, 177 (1995).
24. M. Keim, E. Arnold, W. Borchers, U. Georg, A. Klein, R. Neugart, L. Vermeeren, R. E. Silverans, and P. Lievens, Nucl. Phys. **A586**, 219 (1995).
25. D. Vautherin, Phys. Rev. C **7**, 296 (1973).
26. E. Chabanat, P. Bonche, P. Haensel, J. Meyer, and R. Schaeffer, Nucl. Phys. **A635**, 231 (1998).
27. M. Beiner, H. Flocard, N. Van Giai, and P. Quentin, Nucl. Phys. **A238**, 29 (1975).
28. N. Van Giai and H. Sagawa, Phys. Lett. **B106**, 379 (1981).

29. S. Yoshida and H. Sagawa, Phys. Rev. C **73**, 044320 (2006).
30. L.-W. Chen, C. M. Ko, and B.-A. Li, Phys. Rev. C **72**, 064309 (2005).
31. A.E.L. Dieperink, Y. Dewulf, D. Van Neck, M. Waroquier, and V. Rodin, Phys. Rev. C **68**, 064307 (2003).
32. A.E.L. Dieperink and P. Van Isacker, Eur. Phys. J . A **32**, 11 (2007).